

Critical Review

The Use of Quantitative Imaging in Radiation Oncology: A Quantitative Imaging Network (QIN) Perspective



Robert H. Press, MD,* Hui-Kuo G. Shu, MD, PhD,*
Hyunsuk Shim, PhD,* James M. Mountz, MD, PhD,[†]
Brenda F. Kurland, PhD,[‡] Richard L. Wahl, MD,[§] Ella F. Jones, PhD,^{||}
Nola M. Hylton, PhD,^{||} Elizabeth R. Gerstner, MD,[¶]
Robert J. Nordstrom, PhD,[#] Lori Henderson, PhD,[#]
Karen A. Kurdziel, MD,** Bhadrasain Vikram, MD,^{††}
Michael A. Jacobs, PhD,^{††} Matthias Holdhoff, MD, PhD,^{§§}
Edward Taylor, PhD,^{||||} David A. Jaffray, PhD,^{||||}
Lawrence H. Schwartz, MD,^{¶¶} David A. Mankoff, MD, PhD,^{##}
Paul E. Kinahan, PhD,*** Hannah M. Linden, MD,^{†††}
Philippe Lambin, MD, PhD,^{†††} Thomas J. Dilling, MD,^{§§§}
Daniel L. Rubin, MD, MS,^{||||} Lubomir Hadjiiski, PhD,^{¶¶¶}
and John M. Buatti, MD^{####}

*Department of Radiation Oncology, Winship Cancer Institute of Emory University, Emory University, Atlanta, Georgia; [†]Department of Radiology, School of Medicine, University of Pittsburgh, Pittsburgh, Pennsylvania; [‡]Department of Biostatistics, Graduate School of Public Health, University of Pittsburgh, Pittsburgh, Pennsylvania; [§]Department of Radiology, Washington University, St. Louis, Missouri; ^{||}Department of Radiology, University of California San Francisco, San Francisco, California; [¶]Department of Neurology, Massachusetts General Hospital and Harvard Medical School, Boston, Massachusetts; [#]Cancer Imaging Program, National Cancer Institute, Bethesda, Maryland; ^{**}Molecular Imaging Program, National Cancer Institute, Bethesda, Maryland; ^{††}Radiation Research Program, Division of Cancer Treatment and Diagnosis, National Cancer Institute, Bethesda, Maryland; ^{##}Department of Radiology and Radiological Science, Sidney Kimmel Comprehensive Cancer Center, Johns Hopkins University, Baltimore, Maryland; ^{§§}Brain Cancer

Reprint requests to: Robert H. Press, MD, Department of Radiation Oncology, 1365 Clifton Rd NE, Suite CT-104, Emory University, Atlanta, GA 30322. Tel: 404-778-3473; E-mail: rhp@emory.edu

Conflict of interest: H-K.G.S. reports grant nos. R01CA214557 and U01CA172027. H.S. reports grant nos. R01CA214557 and U01CA172027. N.H. reports grant nos. P01CA210961-01A1 and R01CA132870. E.G. reports grant nos. R01CA211238-01, K23CA169021-04, and U01CA15460. M.J. reports grant nos. U01CA140204 and 1R01CA190299. J.M. reports grant no. U01CA140230. B.K. reports grant nos. U01CA148131, U01CA140230,

and P30CA047904. D.J. reports Canadian Institutes of Health Research (CIHR) funding reference number 137992. M.H. reports grant no. U01CA172027 and serving as a compensated member of the AbbVie scientific advisory board and Celgene scientific advisory board. L.S. reports grant nos. U01CA211205-01 and R01CA194783-03. D.M. reports grant nos. P30CA016520-41, R01CA211337-01, R33CA225310-01, and P30CA016520. P.K. reports grant no. U01CA148131. H.L. reports grant no. U01CA148131. D.R. reports grant nos. U01CA190214 and U01CA187947. L.H. reports grant no. U01CA179106. J.B. reports grant no. U01CA140206.

Program, Sidney Kimmel Comprehensive Cancer Center, Johns Hopkins University, Baltimore, Maryland; ¹¹¹**Princess Margaret Cancer Centre, University Health Network, Toronto, Canada;**
¹¹¹**Department of Radiology, Columbia University Medical Center, Columbia University, New York, New York;** ²²²**Department of Radiology, University of Pennsylvania, Philadelphia, Pennsylvania;**
³³³**Department of Radiology, University of Washington, Seattle, Washington;** ⁴⁴⁴**Department of Medicine, University of Washington, Seattle, Washington;** ⁴⁴⁴**Department of Radiation Oncology (MAASTRO), GROW-School for Oncology and Developmental Biology, Maastricht University Medical Centre, Maastricht, The Netherlands;** ⁵⁵⁵**Department of Radiation Oncology, H. Lee Moffitt Cancer Center and Research Institute, Tampa, Florida;** ⁶⁶⁶**Department of Radiology, Stanford University, Stanford, California;** ⁷⁷⁷**Department of Radiology, University of Michigan, Ann Arbor, Michigan; and**
⁸⁸⁸**Department of Radiation Oncology, University of Iowa, Iowa City, Iowa**

Received Jan 1, 2018, and in revised form May 25, 2018. Accepted for publication Jun 14, 2018.

Modern radiation therapy is delivered with great precision, in part by relying on high-resolution multidimensional anatomic imaging to define targets in space and time. The development of quantitative imaging (QI) modalities capable of monitoring biologic parameters could provide deeper insight into tumor biology and facilitate more personalized clinical decision-making. The Quantitative Imaging Network (QIN) was established by the National Cancer Institute to advance and validate these QI modalities in the context of oncology clinical trials. In particular, the QIN has significant interest in the application of QI to widen the therapeutic window of radiation therapy. QI modalities have great promise in radiation oncology and will help address significant clinical needs, including finer prognostication, more specific target delineation, reduction of normal tissue toxicity, identification of radioresistant disease, and clearer interpretation of treatment response. Patient-specific QI is being incorporated into radiation treatment design in ways such as dose escalation and adaptive replanning, with the intent of improving outcomes while lessening treatment morbidities. This review discusses the current vision of the QIN, current areas of investigation, and how the QIN hopes to enhance the integration of QI into the practice of radiation oncology. © 2018 Elsevier Inc. All rights reserved.

Introduction

Quantitative imaging (QI) is defined as the extraction of quantifiable radiologic biomarkers from medical images for the assessment of the severity, degree of change, or status of a disease or chronic condition relative to normal (1). Its application in oncology is rapidly expanding for diagnosis, staging, and treatment response assessment (2). The use of quantitative metrics in radiation oncology for treatment planning and response assessment has distinct advantages over subjective imaging metrics by providing deeper insight into tumor macro- and microenvironments, correlating with genomic markers (3), and demonstrating associations with radiation therapy (RT) susceptibility and changes in the microenvironment after RT (4, 5).

The National Cancer Institute (NCI) has recognized the importance of QI by funding the Quantitative Imaging Network (QIN) since 2008 under the Cancer Imaging Program (6). The QIN supports use of QI for clinical decision-making in oncology through the development and validation of tools for standardizing image acquisition, processing, and analysis. These tools use analytical algorithms for data quantification to enable personalized treatment for individual patients and the prediction and monitoring of response to drugs or RT (7).

Radiation oncology is increasingly reliant on both qualitative anatomic-based imaging, such as computed tomography (CT) and T1- and T2-weighted magnetic resonance imaging (MRI), and on QI, such as positron emission tomography (PET), single-photon emission CT, diffusion weighted imaging (DWI), and magnetic resonance spectroscopy (MRS). Although the QIN focuses on a wide range of clinical oncologic applications, there is growing interest in producing QI tools specifically to enhance clinical efficacy within radiation oncology. For example, QI has potential to improve prognostication of response to RT which could facilitate personalized treatment decisions and assist in clinical trial design. Functional QI can better identify disease extension beyond conventional imaging techniques, which has become increasingly important as advancements in RT treatment planning and delivery enable increasingly conformal dose distributions. These imaging advances also can provide technical support for treatment strategies such as heterogeneous “dose painting” based on personalized risk (eg, intratumoral hypoxia) and adaptive treatments based on anatomic or functional responses. Ultimately, QI techniques may feed image-derived quantities directly into patient-specific computations of dose. Therefore, understanding and quantifying image-derived signals are a

priority of the QIN and the radiation oncology community at large.

Tools needed to optimize the use of QI in the RT workflow are currently underdeveloped and incomplete. Many labor intensive and often subjective steps in treatment planning, such as manual contouring of target structures, could be optimized by integrating validated QI parameters, including correction algorithms to diminish the effects of known variables (8) and the development of a quantitative data-substantiated workflow that minimizes errors based on known limitations in the current process (9). Algorithm-driven tools to expedite image analysis through automation specifically to assist the radiation oncologist's clinical decision-making are under development by members of the QIN with the goal to maximize the potential of QI. Additionally, implementation of QI into clinical radiation oncology practice requires sophisticated data management, informatics, and statistical analysis, however due to space considerations these topics will not be addressed in this review.

The QIN endorses the exciting potential of QI to ultimately widen the therapeutic window of RT. In this review, the state of QI in the context of RT design, delivery, and response assessment will be discussed, with an emphasis on ongoing and proposed QIN initiatives related to radiation oncology (10).

CT Imaging

Historically, CT imaging has been the backbone of RT planning, providing 3-dimensional (3D) anatomic information and a reliable spatial platform to quantitatively estimate electron density required for dose calculations. Advances in CT imaging include thin-sliced high-resolution acquisitions; 4-dimensional CT that visualizes respiratory motion and thereby allows for respiratory gating of treatment; and dual-energy CT, in which 2 CT datasets are acquired using different photon spectra (11) to improve both tissue differentiation and quantification of dose calculations for photon (12, 13) and particle therapy (14). Other work is ongoing to use other quantitative CT modalities, such as dynamic contrast-enhanced CT, to improve target delineation in specific instances (eg, vascular lesions), to assess perfusion (15, 16), to assess response to RT and antiangiogenic therapies (17-21), and potentially to predict outcomes after RT (22-24).

In the QIN, there is particular interest in using CT-based quantitation of radiomic features in applications within radiation oncology. This area of bioinformatics uses images as mineable data to develop models that can enhance diagnostic accuracy, prognostic capability, and response prediction (25, 26). Specific to RT, analysis of pretreatment CT-based radiomic features has been used to predict for overall survival and patterns of failure after chemoradiation in both non-small cell lung cancer (NSCLC) and head and neck cancer (HNC) (27-29) and in early staged NSCLC

treated with stereotactic body RT (30-32). More recently, this type of feature analysis has been used to predict for pathologic responses in NSCLC after neoadjuvant chemoradiation (33, 34), and further work is being performed to discern the predictive value of feature differences from pre- to post-RT CT scans (35).

Radiomics applications rely on large data sets and unique analysis tools to evaluate a wide variety of imaging features for clinical relevance. For example, a QIN group from the Dana-Farber Institute tested 440 CT-based features that quantified tumor intensity (ie, Hounsfield units), shape, and/or texture in a CT dataset containing 1019 patients treated with chemoradiation for either NSCLC or HNC. Using a smaller training data set, the authors correlated certain imaging features (eg, intratumor heterogeneity) with gene-expression profiles and clinical outcomes. The selected feature set was confirmed in the validation dataset to be predictive of overall survival and certain molecular expression profiles (29). Other QIN investigations have assessed and confirmed the reproducibility of these features using test-retest analyses (36) and the robustness of image features across various extraction algorithms in a multidisciplinary setting (37).

To improve the efficiency of QI integration into standard workflow, QIN researchers at Stanford University developed a QI informatics platform called the electronic Physicians Annotation Device (ePAD). This program provides the ability to quickly perform lesion measurements and repurpose image data to more easily evaluate QI imaging biomarkers across radiologic studies such as CT scans. The device has been shown to reduce the time needed to evaluate scans (38) and could provide a more efficient platform to validate other QI/radiomic parameters as well as an opportunity for rapid analysis needed for online adaptation of therapy. Segmentation algorithms also could assist radiation oncology workflow by providing reliable and accurate contouring target delineation (eg, of lung nodules) (39). The QIN recently completed the Lung CT segmentation QIN challenge, which compared the accuracy and precision of several segmentation algorithms (40). Another example includes a recently validated semiautomated fluorodeoxyglucose (FDG)-PET-based segmentation algorithm for HNC (9). Further development of these tools could fundamentally affect the workflow of RT treatment planning. Although clinical use of quantitative CT parameters is limited to date, its future potential is easy to envision and remains an active area of research in the QIN. Eventually, these tools may also aid in dose selection based on feature analysis, including evaluation of perfusion and identification of necrosis.

PET Imaging

PET is an inherently quantitative modality because its output is based on the temporal and spatial summation of

individual coincident photons to produce a standardized uptake value (SUV). A wide range of PET radiotracers are available or in development that offer high sensitivity and specificity of numerous in vivo biologic and molecular processes. Currently, only [¹⁸F]-FDG, Na[¹⁸F], ¹⁸fluorocholine, [¹¹C]-choline, and [⁶⁸Ga]-DOTA-octreotate (DOTATATE) are approved by the U.S. Food and Drug Administration for oncologic indications, but many others are being evaluated in clinical trials. Identification of quantifiable imaging biomarkers for a variety of biological processes (eg, metabolism, hypoxia, and proliferation) are of interest to the QIN because of their tremendous potential in personalizing cancer care.

FDG-PET

[¹⁸F]-FDG is the most commonly used PET radiotracer in the clinic. It relies on the correlation of glucose metabolism with the upregulation of glucose transporters in cancer cells and has important roles in patient staging, selection, and RT target delineation in numerous disease sites, including NSCLC (41), small cell lung cancer (42), HNC (43, 44), pancreatic cancer (45), lymphoma (46, 47), anal cancer (48), and rectal cancers (49). However, using [¹⁸F]-FDG PET for fine target delineation is generally limited by its relatively low image resolution of 5 to 10 mm. Target delineation can be affected further based on which segmentation method is used (eg, individual visualization, SUV-threshold, or segmentation algorithms) (50-53). A multi-institutional evaluation of PET segmentation performed by the QIN reported a wide range of volume errors, emphasizing the need for standardized methods in future trials (51). Differences in image acquisition, treatment position, respiratory motion (54), image registration (55), and technical factors with individual scanners also affect eventual SUV-based contours (56). The QIN recently completed the QIN PET Segmentation Challenge, a comparison of PET phantom data sets used to assess the variability of segmentation models, and subsequently derived quantitative analysis results. Final results of this challenge may provide insights into how to improve multi-institutional quantitative PET image analysis performance and emphasize the importance of robust quality assurance during the development of automated PET-based target delineation protocols.

Another important role for PET imaging in radiation oncology is its use in early response assessment. The use of [¹⁸F]-FDG to assess early responses to chemotherapy is well established in the literature (57-62), and similar studies have assessed response to chemoradiation. For example, in NSCLC, [¹⁸F]-FDG PET scans obtained by the fifth week of definitive chemoradiation have demonstrated ability to differentiate responders from non-responders (63, 64) and to predict for overall survival (65). Midtreatment [¹⁸F]-FDG PET scans have demonstrated

similar prognostic ability after chemoradiation in other cancers, including cervical cancer (66, 67), rectal cancer (68), and HNC (69). Figure 1 shows an example of tumor FDG-uptake quantification at different time points during treatment.

At this time, the utility of [¹⁸F]-FDG PET response assessment after RT alone is less clear. Trials have reported predictive SUV changes after chemoradiation but not after RT alone (68), suggesting that, in some cases, the predictive metabolic changes may be driven primarily by the chemotherapy component. In addition, the interpretation of SUV changes after RT can be confounded by radiation-induced normal tissue inflammation affecting [¹⁸F]-FDG uptake. In vitro studies show early flares in FDG uptake in tumor cells, followed by response, but such changes are less frequent in vivo (70). Given the accumulation of inflammation throughout a radiation course, the optimal timing for assessment will be important to establish in future studies. Despite these limitations, there remains great enthusiasm for early PET assessments in radiation oncology, and QIN investigators continue to examine an increasing role for [¹⁸F]-FDG PET in this capacity.

An exciting application of this strategy is the use of a midtreatment [¹⁸F]-FDG PET scan as a functional biomarker to facilitate adaptive dose escalation to poorly responding disease. Kong et al recently conducted a phase II PET-adapted RT trial for patients with NSCLC (N = 42) undergoing chemoradiation using interim [¹⁸F]-FDG PET at 45 Gy to identify regions of poorly responding disease, which were then targeted up to 86 Gy (71). The 2-year infield disease control rate of 82% was a considerable improvement from Radiation Therapy Oncology Group (RTOG) 0617, which had a 2-year infield control rate of 61% to 69%. Given these promising results with PET-adapted dose escalation, this strategy is now the basis for RTOG 1106, a phase II randomized trial that has accrued fully and is awaiting initial analysis. An example is shown in Figure 2 demonstrating the predictive value of mid-treatment [¹⁸F]-FDG PET. There are several ongoing clinical trials that include early response assessment in rectal cancer (NCT02233595, University of California, San Francisco) and glioblastoma (NCT02902757, University of California, Los Angeles) and early response assessment with adaptive replanning in NSCLC (NCT02773238, University of Washington; NCT02492867, University of Michigan).

An important hurdle that must be addressed before the implementation of FDG-based parameters to dictate treatment decisions and define target volumes in multicenter clinical trials is the need to standardize scanner output, segmentation methods, and analysis tools (72). For example, inherent variability in adjusted [¹⁸F]-FDG PET SUV from individual scanners can range over 20% (73), but QIN investigators at the University of Washington reduced error to less than 4% using routine calibration protocols (74). Deviations in the time between radiotracer injection

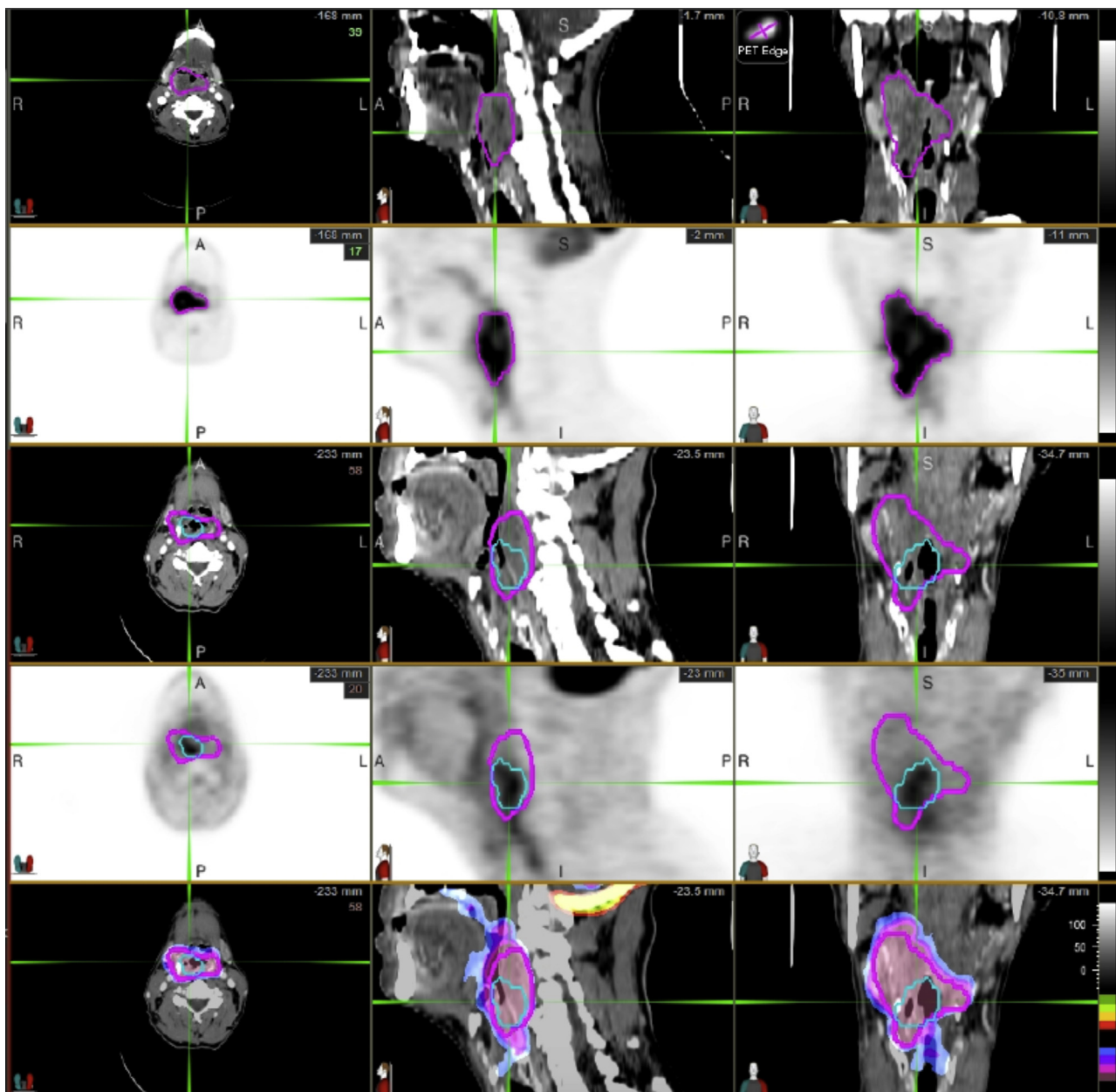


Fig. 1. FDG-PET demonstrates the ability to quantify gross tumor metabolic volume at baseline and after radiation therapy for the purposes of assessing response and to provide a predictive biomarker of early therapeutic efficacy. Rows 1 and 2: Baseline PET/CT—The magenta is the lesion volume of interest, which was automatically generated based on PET intensity gradients. Rows 3 and 4: Follow-up PET/CT—Magenta is original volume of interest deformed to match the patient's anatomy on follow-up CT image. Blue is the lesion volume of interest automatically generated based on PET intensity gradients in the follow-up PET image. Row 5: Color-coded normalized SUV voxel-by-voxel subtraction fused with CT. This allows a full 3-dimensional comparison of regions of response and nonresponse in a large heterogeneous tumor. (A color version of this figure is available at <https://dx.doi.org/10.1016/j.ijrobp.2018.06.023>.)

and image acquisition and multiple other factors also can affect SUV values, suggesting the need for stricter imaging protocols (75). Guidelines have been published to help standardize image acquisition procedures (76). QIN groups at the University of Washington and the University of Iowa are actively working on both processing tools to improve consistency and standardize protocols to limit output

variations across institutions (77). To address the need for broader standardization, the University of Washington group developed the software program F-18 X-Cal System, which allows for cross-calibration of PET scanners, dose calibrators, and well detectors for Ga-68 and [¹⁸F] isotopes in a multicenter setting. These steps to limit sources of error may improve the sensitivity of trials investigating QI-based

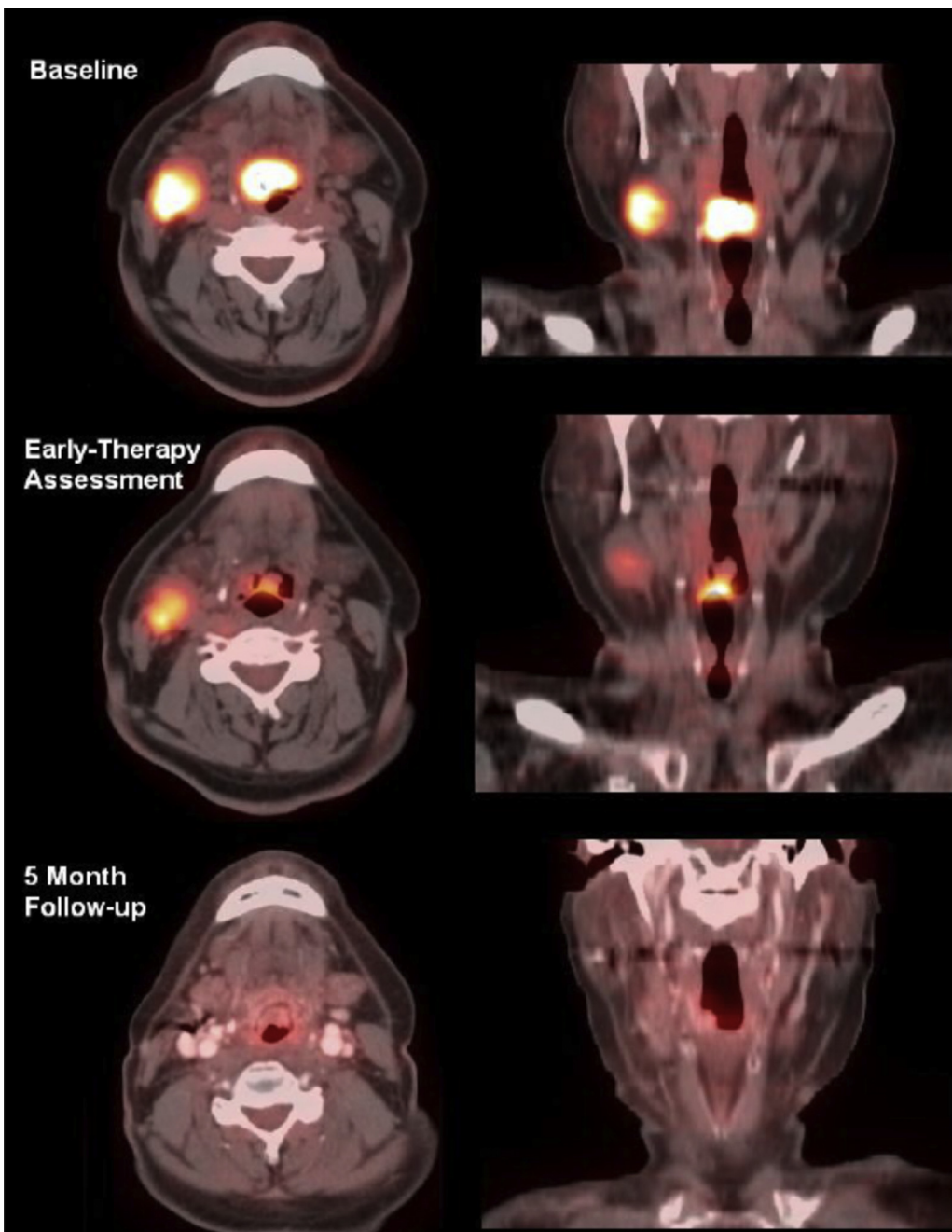


Fig. 2. FDG-PET/CT images of 57-year-old man with base-of-tongue squamous cell carcinoma and a right level 2 cervical metastasis undergoing therapy. The PET intensity gradient tool shown in Figure 1 was used to generate total glycolytic volumes at baseline, early during therapy, and posttreatment. [18F]-FDG uptake between baseline and an early response assessment time (day 21) was significantly reduced, with tumor glycolytic index decreasing from 87.6 standard uptake volume-mL (SUV-mL) to 19.3 SUV-mL. At 5-month follow-up, the patient showed an excellent response with near complete interval resolution of disease. Primary tumor uptake was reduced to background levels, with a measured tumor glycolytic index of 7.0 SUV-mL. Nodal metastasis also had good therapy response. This figure illustrates that an early reduction in total glycolytic volume can be used as a predictive biomarker. In this case, the large reduction in total glycolytic volumes at 3 weeks was predictive for a beneficial longer-term outcome.

PET biomarkers. As standardization protocols evolve, further refinement of accreditation standards for imaging centers to participate in QI clinical trials will be needed (78, 79).

Postacquisition analysis and response interpretation is another step that warrants further evaluation. Image processing algorithms across vendors and institutions are currently heterogeneous and will require standardization to

ensure comparable data analysis. General guidelines have been published to standardize the interpretation of post-treatment PET responses, including the European Organization for Research and Treatment of Cancer (EORTC) (80) and later the PET Response Criteria in Solid Tumors (PERCIST) criteria with input by the NCI (81). However, a limitation to incorporating PERCIST criteria into detailed response assessments has been the lack of integrated workflow tools. To improve automation of PERCIST criteria, QIN investigators at Johns Hopkins University and Washington University in St Louis have been involved in the development and evaluation of the computer software Auto-PERCIST (82). Automatic processes will allow for computer-aided analysis, database integration, and automated report generation (9). In radiation oncology, a future potential application of these automatic platforms could be the rapid integration of FDG-SUV values into RT planning software, which may assist in factors ranging from the objective characterization of nonresponding tissues to decision-making regarding RT boost volumes. Of note, the SUV normalized for lean body mass (SUL) peak parameter is emphasized in the Auto-PERCIST formulation because of strong correlations between absolute SUV and body weight, which proper correction to lean body mass minimizes (83). In addition, SUL peak values are less subject to noise-induced upward bias than are SUV max values (84). Thus, when SUV-based cut-offs are used, close attention must be paid to the specific quantitative metric applied and the reconstruction parameters (85). SUL peak formulations are increasingly recognized as more stable.

Hypoxia PET

Tumor hypoxia is a known cause of radioresistance and can vary widely among different individual tumors and tumor types (86). Traditional measurements of tumor hypoxia require direct *in vivo* probes or biopsy (87), but the development of PET radiotracers (eg, [¹⁸F]-fluoromisonidazole (88), [¹⁸F]-fluoroazomycin arabinoside (89, 90), [¹⁸F]-flortanidazole (91), and Cu-ATSM (92)) now allows for noninvasive visualization of various hypoxic processes. Tumor hypoxia is often heterogeneous (93, 94), implying that certain tumor subvolumes are more hypoxic and, therefore, more radioresistant. Numerous prospective studies involving HNC (95-97), glioblastoma (98, 99), NSCLC (100, 101), cervix (102), and prostate (103) report worse local control and overall outcomes for hypoxic tumors after RT. Tumor hypoxia also has been shown to be dynamic during RT (104), especially early in treatment, indicating that reoxygenation could be used as an early biomarker (97).

In radiation oncology, 2 open trials from Memorial Sloan Kettering are examining the prognostic capability of [¹⁸F]-MISO PET in rectal cancer (NCT00574353) and NSCLC (NCT02016872) after RT. In addition, there is great interest in using hypoxia PET to apply RT dose

painting to intensify the dose to hypoxic areas (105, 106). A phase II trial in HNC has reported improved locoregional control (107), and this strategy is being further investigated in the German phase III ESCALOX trial (NCT01212354) (108). Adaptive strategies are also under investigation, including a recently accrued phase II trial at Stanford University (NCT01507428) that is assessing the utility of midtreatment [¹⁸F]-MISO PET in NSCLC.

Similar to [¹⁸F]-FDG PET, hypoxia imaging protocols will need to be standardized to guide clinical trial design with hypoxia PET radiotracers. A Canadian QIN group from Princess Margaret Cancer Centre/University Health Network in Toronto is working to standardize acquisition methodology, integrate other imaging methods to produce a more robust tracer kinetic model, and develop software to make analysis of quantitative hypoxia metrics more facile (109). These efforts will be shared through the QIN to facilitate multi-institutional retrospective studies containing hundreds of hypoxia imaging datasets. In addition, a major challenge to the clinical utility of hypoxia PET imaging compared with other tracers, such as FDG, is the small signal-to-background ratio of all known agents. It is therefore crucial to develop hypoxia PET imaging biomarkers that exhibit heightened sensitivity to hypoxia relative to background tissue and that can be measured reproducibly across different sites. Important questions that are being addressed to achieve this goal include the choice of optimal reference tissue (eg, blood or muscle) (110, 111), the choice of threshold for hypoxic status determination, and the need for dynamic PET modeling to correct for tumor transport properties (ie, background) (112-114). Ongoing trials seek to validate PET-hypoxia imaging biomarkers against postresection pathology in pancreatic cancer (NCT01542177) and assess their prognostic capabilities in cervical cancer (NCT01549730).

Proliferation PET

Imaging cellular proliferation is of intuitive interest to oncologists. [¹⁸F]-fluorothymidine (FLT) is a PET tracer that relies on the upregulation of the enzyme thymidine kinase 1 during the S-phase of the cell cycle. Thymidine kinase 1 phosphorylates FLT, which fixes it intracellularly and leads to accumulation in rapidly proliferating cells (115). [¹⁸F]-FLT has several potential advantages over [¹⁸F]-FDG, particularly for use after RT. First, [¹⁸F]-FLT PET has been shown to quantify similar SUVs across multiple institutions with excellent repeatability (116). Second, [¹⁸F]-FLT PET measures may be more specific in assessing response to RT because they are associated with a cellular process directly related to cell proliferation rather than glycolysis, the latter of which may be upregulated in both active tumor and normal areas with radiation-induced inflammation. This theory is supported by comparative studies of [¹⁸F]-FLT and [¹⁸F]-FDG. For example, [¹⁸F]-FLT PET has demonstrated greater success in identifying pathologic complete

response after chemoradiation in patients with rectal cancer (117). Additionally, in contrast to [¹⁸F]-FDG, decreases in [¹⁸F]-FLT SUV have shown predictive value after RT alone (118). Together, these advantages suggest a wider potential utility of [¹⁸F]-FLT PET in radiation oncology. These advantages, however, must be balanced against the lower absolute SUV of [¹⁸F]-FLT in many cancers. Comparative studies after chemotherapy alone have reported worse predictive value of [¹⁸F]-FLT compared with [¹⁸F]-FDG (119), indicating the need for caution until further treatment-specific studies are available.

A major area of interest for use of [¹⁸F]-FLT PET is in early response assessment during RT. Studies have evaluated this strategy in HNC and NSCLC and generally demonstrated improved tumor control with decreasing [¹⁸F]-FLT uptake (120-122). However, a recent study by Everitt et al conversely reported that stable uptake of [¹⁸F]-FLT at week 2 of chemoradiation for NSCLC was associated with improved overall survival compared with complete or partial FLT response. The authors hypothesized that reduced [¹⁸F]-FLT uptake may have been associated with suppression of tumor cell proliferation, resulting in decreased RT-induced tumor cell mitotic death and, consequently, worse overall outcomes. This finding has important implications because it indicates potentially disparate kinetic responses between radiotracers and emphasizes the need to validate biomarkers before clinical implementation (122).

Another potential role for [¹⁸F]-FLT PET is to differentiate tumor progression from treatment effect after RT. This ability is being investigated in prospective trials for both brain metastases (NCT02328300) and NSCLC (NCT02456246). QIN researchers at the University of Iowa have also investigated use of [¹⁸F]-FLT PET to identify and avoid active (ie, proliferating) bone marrow in patients when optimizing RT treatment plans. Implementing this strategy has been shown to reduce the risk of leukopenia in patients with pelvic malignancies, supporting this novel use as a strategy to reduce treatment toxicity (123).

Non-FDG metabolism PET

Numerous other radiotracers in addition to FDG have been studied to exploit the inherent increased metabolic demands within tumors. Choline (Cho) is an essential nutrient required for Cho phospholipid metabolism (124). Amino acid tracers, which rely on increased anabolic demands and increased amino acid transport via LAT1 and LAT2, are also under investigation. They appear particularly useful for intracranial disease and include [¹¹C]-methionine and 18-fluoroethyl-tyrosine.

Several promising PET tracers specific to prostate cancer have been developed (125). Prostate-specific membrane antigen (PSMA) is a semiquantitative tracer that can be used in systemic staging and in guidance for salvage RT in the setting of recurrences (126). In addition, anti-1-amino-3-¹⁸F-fluorocyclobutane-1-carboxylic acid (FACBC) is a

synthetic l-leucine analog that has demonstrated high uptake in prostate cancer cells (127) and may play an important role for RT treatment planning. A NCI-sponsored randomized trial is ongoing to assess the clinical significance of using FACBC-PET during RT treatment planning (NCT01666808). A current limitation of these modalities is the semiquantitative method for volume segmentation. The development of formal segmentation methods would be clinically useful.

PET radiomics

In combination with CT-based radiomic analysis, PET data can be mined to discern clinically relevant information (128). For example, PET imaging biomarkers have been reported to correlate with underlying genomic phenotypes (129) and somatic mutation patterns (130) to better predict clinical outcomes and direct treatment decisions. Other clinical studies have suggested PET-based radiomic analyses add predictive value to [¹⁸F]-FDG PET in HNC (131), rectal cancer (132), and cervical cancer (133). Textural analysis (eg, coarseness) of 18-fluoroethyl-tyrosine PET scans along with conventional imaging have also demonstrated improved diagnostic accuracy in discerning radiation necrosis from tumor progression in brain metastases, suggesting its ability to enhance diagnostic discrimination after RT (134). QIN investigators from the Dana Farber Cancer Institute at Harvard University are developing radiomic analysis systems to correlate PET/CT imaging features and genomic profiling to non-invasively assess molecular features and monitor treatment responses.

A major issue for PET-based radiomic analyses involves the varying output of textural features on which the SUV segmentation method is based. There appears to be poor reliability between different analysis methods (135) and a lack of reproducibility between features (131). The standardization of these methodologies will be critical to properly interpreting textural results, and the minimization of such analytical variance remains a priority of the QIN.

MRI

MRI is a widely used imaging modality with distinct ability to provide increased soft tissue contrast with high spatial and temporal resolution. The importance of MRI in radiation oncology continues to grow as treatment planning becomes more dependent on reliable delineation of targets and organs at risk. This reliance will likely continue to grow stronger as linear accelerator systems become integrated with MRI to provide live high-resolution image guidance and facilitate adaptive replanning. Anatomic MRI scans are primarily T1- and T2-weighted sequences that can delineate normal from abnormal tissue. These MRI scans can be obtained with fat or nonfat saturation pulse

sequences to highlight different tissue types. Advanced MRI sequences—including perfusion, DWI with apparent diffusion coefficient (ADC) mapping, diffusion tensor imaging (DTI), and spectroscopy—can provide additional quantitative molecular and biological information in parallel with the highly detailed anatomy of routine T1/T2 sequences. QIN members are involved with several studies assessing the clinical utility of these techniques and broadly pursuing tools to advance the incorporation of quantitative MRI in radiation oncology. Quantitative MRI could assist greatly in patient selection, tumor delineation, prediction of RT response, planning adaptation, and improved assessment of overall treatment response.

Perfusion MRI

Perfusion-weighted MRI sequences can interrogate the vascularity of tissue and other parameters related to perfusion. This modality leverages the frequently increased vascularity of tumors resulting from abnormal angiogenesis to provide insights into tumor biology. The 2 most common methods of perfusion MRI are dynamic contrast enhanced (DCE) MRI and dynamic susceptibility contrast (DSC) MRI. These methods quantify changes in tissue contrast over time by acquiring rapid MRI sequences before, during, and after intravenous injection of a gadolinium-based contrast agent. For DCE-MRI, dynamic T1-weighted images are obtained, and changes in contrast signal are quantified. A variety of microvascular environment parameters can be calculated by fitting time-contrast intensity curves (or time-contrast agent concentration curves) to different pharmacokinetic (PK) models. Standard quantitative PK parameters for DCE-MRI include (1) K_{trans} , the volume transfer constant between blood plasma and the extracellular, extravascular space; (2) K_{ep} , the redistribution rate constant from the extracellular, extravascular space to the blood plasma; and (3) V_p and V_e , the plasma and extracellular, extravascular volume fractions, respectively (136). For DSC-MRI, dynamic T2- or T2*-weighted sequences are obtained before and after a contrast bolus. The changes in T2 or T2* relaxation times are measured and applied to PK models to estimate different hemodynamic parameters, including cerebral blood volume (CBV), cerebral blood flow, and mean transit time.

Clinical appreciation of the characterization of vascular parameters is rapidly expanding. For intracranial malignancies, perfusion parameters obtained from DSC (137, 138) and DCE (139–141) MRI scans have demonstrated excellent ability to differentiate radiation necrosis from tumor progression. Comparative studies of the 2 methods have been reported (142), and further investigation is needed to identify optimized parameters and modality combinations. A study investigating DCE CT and DCE MRI for brain metastases after stereotactic radiosurgery reported high correlations if the same analysis platform is used (16). Studies have also demonstrated the value of

early changes in perfusion MRI to predict for survival outcomes. American College of Radiation Imaging Network (ACRIN) 6677/RTOG 0625 reported that early decreases in the relative CBV were associated with improved 1-year survival in patients with recurrent glioblastoma (143). Based on this finding, ECOG-ACRIN initiated a phase II trial (NCT03115333) in which patients with recurrent glioblastoma are treated with bevacizumab and imaged with early DSC-MRI scans (2 weeks post-therapy) to determine whether early relative CBV response correlates with overall survival. These projects highlight the QIN collaboration with ECOG-ACRIN (144), which will expand the translational reach of the QIN and carry its expertise into working group platforms of national cooperative groups. This partnership seeks to improve the value, effectiveness, and efficiency of clinical trials while also validating QI-based imaging parameters in the prospective setting. In this collaboration, the QIN anticipates an expansion of radiation-focused, QI-based trials.

The QIN also has a particular interest in the use of perfusion MRI to detect treatment-resistant regions of disease and provide guidance for adaptive RT dosing. For example, in patients with HNC treated with chemoradiation, early increases in vascularity identified on DSC-MRI have demonstrated ability to predict tumor responses (145), suggesting increased oxygen availability may correlate with tumor radiosensitivity. DCE-MRI K_{trans} values correlating with tumor heterogeneity also have been associated with greater radioresistance in HNC (146, 147), glioblastoma (140), NSCLC (148), and rectal cancer (149). QIN members are actively using these modalities to identify subvolumes at greater risk of local failure (150) and attempting to integrate dose escalation strategies into clinical trials. This paradigm is highlighted by an ongoing randomized phase II trial by QIN researchers at the University of Michigan, in which dose painting to hypoperfused subvolumes in locally advanced HNC based on DCE-MRI is performed (NCT02031250). In conjunction with this trial, steps are under way to improve the standardization of volume delineation across scanners and automation of these analyses (151). The QIN is also rigorously assessing the robustness of MRI-based QI parameters through quality assurance studies (152) and endeavors such as the QIN-sponsored arterial input function challenge (153).

DWI with ADC mapping

DWI is a non-contrast enhanced sequence that generates images used to assess the rate of water diffusion. Successive images are obtained using varying diffusion gradients to estimate an ADC map. In cancer, restricted diffusion is caused by hypercellularity and quantified by a low ADC map value. If there are changes in the tumor, such as cell death or treatment effect, the ADC value typically increases.

Given that DWI/ADC mapping can identify fine changes in cellular density before apparent anatomic differences occur (154), its utility for assessing early responses to RT is of significant interest. Studies have reported using this strategy for intracranial malignancies (154), HNC (155), esophageal cancer (156), and prostate cancer (157). Numerous clinical trials are ongoing which incorporate DWI/ADC mapping in this fashion, including in esophageal cancer (NCT03151642), HNC (NCT02497573, NCT00581906), prostate cancer (NCT02319239), rectal cancer (NCT02233374), pediatric sarcoma (NCT02415816), and cervical cancer (NCT01992861). DWI/ADC mapping also has been used to discern recurrences from radiation effect after RT (158–162). Often these analyses are performed in combination with [¹⁸F]-FDG PET (160) or other multiparametric MRI modalities (161, 162).

Additionally, wider availability of 3T MRI with more powerful gradient subsystems now allows for clinical use of high b-values for DWI while maintaining adequate signal-to-noise ratios, which is not typically possible using 1.5T MRI scanners. High b-values provide better image contrast and tissue diffusivity measurements, result in less T2 shine-through effect, and allow less conspicuous features to be observed (163). In prostate cancer, high b-value DWI (most commonly in the setting of multiparametric MRI) has been reported to better identify malignant lesions (163–165), predict Gleason grade (166, 167), and identify extracapsular extension (168). Interestingly, manual interpretation has been reported to be superior to region of interest–based ADC values (165), emphasizing the need for improved quantitative metrics.

In addition to validating both histogram and voxel-based DWI/ADC metrics as clinical biomarkers, QIN investigators at the University of Michigan are actively pursuing a standardized acquisition platform for ADC mapping. Similar to the needs of other QI modalities, robust quality assurance and standardization of system performance metrics across scanner vendors will be needed to improve comparability (169). There is also promise for advanced image segmentation and image feature analyses to broaden the capabilities of DWI.

MRS

MRS is a quantitative molecular-based technique that measures the levels of metabolites within tissue. MRS data can be either in single-voxel or multivoxel mode, with multivoxel data acquired using magnetic resonance spectroscopic imaging (MRSI). In contrast to other magnetic resonance modalities, MRSI provides a voxel-based spectrum of resonance “peaks” rather than an image and is obtained in conjunction with anatomic MRI sequences to spatially correlate with regions of interest. MRSI detects the frequency of various metabolites by nuclear magnetic resonance, most commonly of ¹H in units of parts per

million (ppm). The most common metabolites are N-acetyl aspartate (NAA), a neuronal metabolite and marker at 2.2 ppm; creatine/phosphocreatine (Cr), a marker of energy metabolism at 3.0 ppm; and Cho, a measure of cell membrane turnover (tumor activity) at 3.2 ppm. Spectra examples for glioblastoma and contralateral normal brain are shown in Figure 3A.

Significant effort has been made to use MRSI in brain tumors. Spectroscopy metrics have demonstrated ability to differentiate tumor grade (170), and increases in certain metabolites and their ratios, such as Cho-to-NAA ratio (Cho/NAA), lipid, and lactate, during treatment have been associated with worse outcomes and the sites of local recurrences (171–173). During posttreatment surveillance, MRSI has been reported to improve specificity between tumor progression and radiation necrosis. However, for small tumors, this technique has limited sensitivity (174).

In addition, for infiltrative brain malignancies such as glioblastoma, a promising use of MRSI includes integrating metabolite profiles to better define microscopic disease extension. In one study, regions with pretreatment Cho/NAA ratios ≥ 2 predicted for sites of contrast-enhancing recurrence, often in regions not originally targeted by conventional volumes (175). Studies are now integrating MRSI into RT planning to optimize tumor coverage (172,173,175–179). QIN investigators at Emory University are advancing the use of spectroscopy for this purpose using a recently developed echo planar spectroscopic imaging sequence, called spectroscopic MRI (sMRI), that achieves 3D whole brain coverage at relatively high resolution (nominal voxel size of ~ 5 mm). This group reported that abnormal pretreatment sMRI volumes predicted for the sites of eventual glioblastoma recurrence, and the retrospective integration of these abnormal volumes (defined at Cho/NAA thresholds of 1.5, 1.75 and 2.0 greater than contralateral white matter) into the original treatment plans would have improved coverage of the recurrent disease (92.4%, 90.5%, and 88.6%, respectively) compared with the original treatment (82.5%) while maintaining dosimetric constraints (177). An example is shown in Figure 3B demonstrating regions of disease recurrence that were previously identified by pretreatment Cho/NAA maps despite not being apparent on the initial T1 postcontrast or fluid attenuation inversion recovery (FLAIR) sequences. A phase II trial at Emory University and Johns Hopkins University has been initiated that prospectively examines the predictive value of serial 3D whole brain sMRI for patients with newly diagnosed glioblastoma treated with the histone deacetylase inhibitor belinostat along with standard RT and temozolomide (NCT02137759).

With an improved ability to identify volumes at high risk of containing subclinical disease several clinical trials are utilizing MRSI to guide selected dose escalation. Using a simultaneous integrated boost up to 72 Gy was reported to be dosimetrically feasible (180), and this strategy is now the basis for the SPECTRO GLIO trial, a French

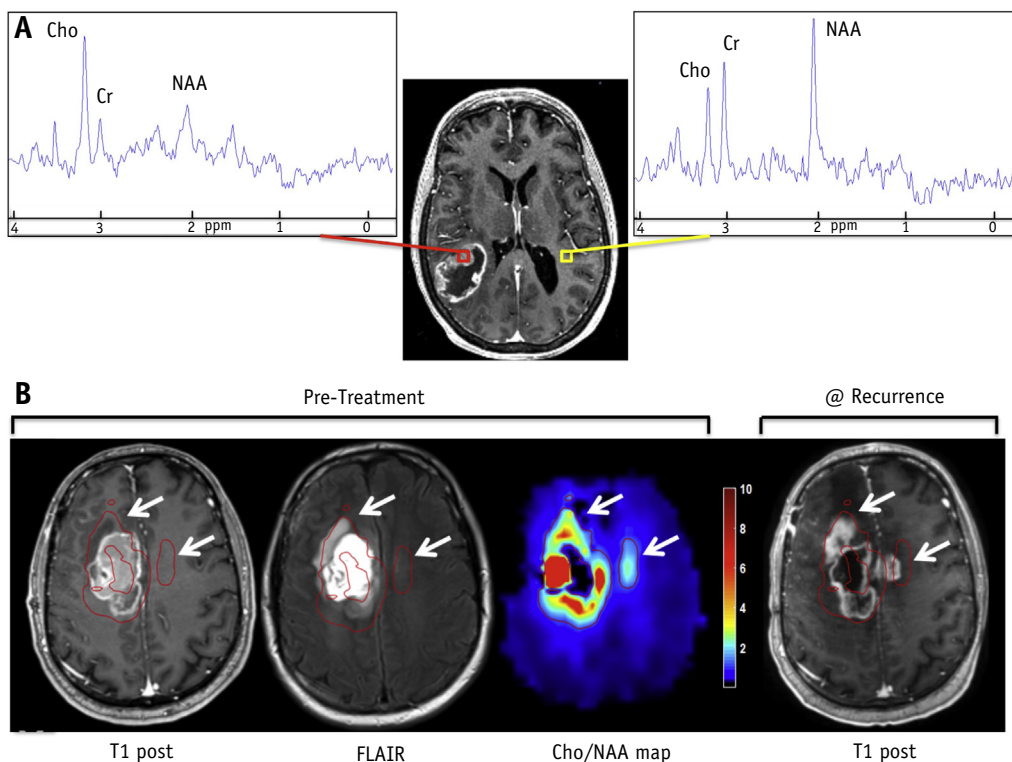


Fig. 3. (A) Spectra from voxels representing glioblastoma (red) or contralateral normal brain (yellow) from a whole brain echo planar spectroscopic imaging (EPSI) acquisition are shown. Choline (Cho), (creatine) Cr, and N-acetylaspartate (NAA) peaks are indicated. (B) Pretreatment anatomic (T1 postcontrast and FLAIR), spectroscopic (Cho/NAA map from whole brain EPSI) sequences, a T1 postcontrast sequence obtained 5 months after radiation therapy of a glioblastoma case are shown. All sequences were matched using a rigid registration algorithm. Cho/NAA ratio values are normalized to an average of the normal contralateral white matter Cho/NAA values and presented as a color wash map. A cutoff normalized Cho/NAA value of 2.0 is used to generate the red contours that are shown, indicating high-risk regions based on the Cho/NAA map. White arrows denote regions deemed high risk by Cho/NAA map that ultimately failed with contrast-enhancing disease but showed no evidence of abnormal signal on the pretreatment T1 postcontrast or FLAIR sequences. (A color version of this figure is available at <https://dx.doi.org/10.1016/j.ijrobp.2018.06.023>.)

randomized phase III study comparing the standard of care with or without a simultaneous integrated boost to 72 Gy directed at the volume defined by a Cho/NAA ratio >2 and T1 postcontrast enhancement (NCT01507506). In the United States, the Emory QIN group is leading a single-arm, multisite pilot study to assess the feasibility and progression-free survival benefit of dose escalation to 75 Gy using a similar high-risk volume identified on 3T 3D whole brain sMRI (NCT03137888).

MRSI is also under investigation in prostate cancer. Normal prostate tissue typically contains high levels of citrate (2.6 ppm) and Cr and low levels of Cho. Ratios of Cho-to-citrate and Cho+Cr-to-citrate may be helpful in distinguishing normal from malignant tissue and assist with biopsy planning (181). Molecular atrophy, defined by Cho and citrate peak area-to-noise-ratio $<5:1$, is known to occur after RT and negatively correlates with PSA levels and response (182). After RT, addition of MRSI to T2-weighted MRI improved the diagnostic accuracy of questionable recurrent lesions (183). Furthermore, the total Cho-to-Cr ratio (tCho/Cr) from

biopsy samples was reported to predict high-risk versus indolent disease (2.4 ± 0.4 vs 1.5 ± 0.2) with an accuracy of 95% and may help stratify individual risk and select patients in need of salvage therapy (184). Additionally, because local failure after RT most commonly occurs in dominant intra-prostatic lesions (185), image guided dose escalation has drawn significant interest (186). Reports using MRSI to guide brachytherapy dose escalation have reported excellent clinical outcomes and toxicity rates (187, 188), and this may be an important strategy for patients with unfavorable-intermediate or high-risk disease.

MRI Radiomics and Segmentation

Given the wide range of available textural information, multiparametric MRI-based radiomic feature analysis has tremendous potential to provide insights beyond quantified signal intensity. Numerous QIN teams spearheaded by the group at Johns Hopkins University are working to extract

and validate robust radiomic features for clinical use. Initial work has evaluated feature profiles to discern benign from malignant lesions (189), identify radiation necrosis after RT (190, 191), generate automatic tumor segmentation algorithms (192, 193), and improve prognostic capabilities in glioblastoma after chemoradiation (194, 195). An interesting example of this approach was pursued by researchers at the University of Heidelberg, where 181 multiparametric MRI scans of patients with glioblastoma were analyzed. From these scans, 1043 imaging features were extracted. Reproducible image characteristics were identified using test-retest analyses and subsequently modeled on a discovery cohort to identify a specific radiomic signature predictive for progression-free and overall survival. This identified signature was then tested in a multivariate Cox model using a validation cohort and found to be independently associated with outcomes in addition to MGMT methylation (195).

Deep-learning feature extraction is also being conducted to recognize patterns specific to genomic phenotypes (196–198). In prostate cancer, regions of abnormal radiomic features pathologically confirmed via targeted prostate biopsies were able to discern various gene expression patterns involved in immune and inflammatory response, metabolism, and cell and biological adhesion (196). Strategic platforms integrating radiomic information into RT treatment planning are now under development, such as “Radiomics based targeted radiotherapy planning” (Rad-TRaP) developed by researchers at Case Western Reserve University (199). The program generates radiomic-based brachytherapy dosing or external beam plans based on lesions identified by feature analysis on multiparametric MRI scans, and demonstrated ability to reduce dose to organs at risk while delivering boosts to the identified lesions. Further automation has the exciting potential to streamline radiation oncology workflow while enhancing clinical care. The QIN remains committed to advancing these endeavors with the development of imaging processing platforms that facilitate the discovery and validation of radiomic biomarkers.

Conclusions

A wide range of radiologic QI modalities is being investigated to better characterize tumor characteristics and to assess radiation treatment effects and outcomes. These quantitative assessments complement the traditionally qualitative use of standard imaging methods. The rapid development of radiologic biomarkers using QI analysis tools for clinical decision-making is promising, and subsequent integration into daily radiation oncology practice is expected. To do so, however, will require the field to invest in rigorous quantification and validation. The most common applications for these tools are for treatment planning, risk stratification, guidance of dose escalation, and characterization of posttreatment effects. By collaborating

across disciplines in a unified goal-oriented network, the QIN seeks to address the challenges of integrating QI into the radiation oncology clinical workflow, including identification and standardization of clinically significant QI parameters and optimization of existing imaging methods for RT planning and response assessment. These important investigations are necessary for the robust integration of individual patients’ anatomic, biological, physiological, and genomic imaging characteristics into radiation oncology decision-making and treatment design, thereby enabling truly personalized cancer care.

References

1. Radiological Society of North America. Quantitative Imaging Biomarkers Alliance (QIBA). Available at: <http://www.rsna.org/QIBA/>. Accessed December 1, 2017.
2. Yankelev T, Mankoff DA, Schwartz LH, et al. Quantitative imaging in cancer clinical trials. *Clin Cancer Res* 2016;22:284-290.
3. Keam SP, Caramia F, Garnell C, et al. The transcriptional landscape of radiation-treated human prostate cancer: Analysis of a prospective tissue cohort. *Int J Radiat Oncol Biol Phys* 2018;100:188-198.
4. Filatenkov A, Baker J, Mueller AMS, et al. Ablative tumor radiation can change the tumor immune cell microenvironment to induce durable complete remissions. *Clin Cancer Res* 2015;21:3727-3739.
5. Filatenkov A, Baker J, Strober S. Disruption of evasive immune cell microenvironment in tumors reflects immunity induced by radiation therapy. *Oncoimmunology* 2016;5:e1072673.
6. National Cancer Institute Cancer Imaging Program. Quantitative Imaging Network. Available at: <http://imaging.cancer.gov/informatics/qin.htm>. Accessed December 1, 2017.
7. Jaffray DA, Chung C, Coolens C, et al. Quantitative imaging in radiation oncology: An emerging science and clinical service. *Semin Radiat Oncol* 2015;25:292-304.
8. Bauer C, Sun S, Sun W, et al. Automated measurement of uptake in cerebellum, liver, and aortic arch in full-body FDG PET/CT scans. *Med Phys* 2012;39:3112-3123.
9. Beichel RR, Van Tol M, Ulrich E, et al. Semiautomated segmentation of head and neck cancers in 18F-FDG PET scans: A just-enough-interaction approach. *Med Phys* 2016;43:2948-2964.
10. National Cancer Institute Cancer Imaging Program. About the Quantitative Imaging Network (QIN). Available at: https://imaging.cancer.gov/programs_resources/specialized_initiatives/qin/about/teams.htm. Accessed December 1, 2017.
11. Johnson TR. Dual-energy CT: General principles. *Am J Roentgenol* 2012;199:S3-S8.
12. Yamada S, Ueguchi T, Ogata T, et al. Radiotherapy treatment planning with contrast-enhanced computed tomography: Feasibility of dual-energy virtual unenhanced imaging for improved dose calculations. *Radiat Oncol* 2014;9:168.
13. Bazalova M, Carrier J, Beaulieu L, et al. Dual-energy CT-based material extraction for tissue segmentation in Monte Carlo dose calculations. *Phys Med Biol* 2008;53:2439-2456.
14. Hunemohr N, Krauss B, Tremmel C, et al. Experimental verification of ion stopping power prediction from dual energy CT data in tissue surrogates. *Phys Med Biol* 2014;59:83-96.
15. Jensen NK, Mulder D, Lock M, et al. Dynamic contrast enhanced CT aiding gross tumor volume delineation of liver tumors: An interobserver variability study. *Radiother Oncol* 2014;111:153-157.
16. Coolens C, Driscoll B, Foltz W, et al. Comparison of voxel-wise tumor perfusion changes measured with dynamic contrast-enhanced (DCE) MRI and volumetric DCE CT in patients with metatstatic brain cancer treated with radiosurgery. *Tomography* 2016;2:325-333.

17. Fraioli F, Anzidei M, Zaccagna F, et al. Whole-tumor perfusion CT in patients with advanced lung adenocarcinoma treated with conventional and antiangiogenetic chemotherapy: Initial experience. *Radiology* 2011;259:574-582.
18. Cao N, Cao M, Chin-Sinex H, et al. Monitoring the effects of anti-angiogenesis on the radiation sensitivity of pancreatic cancer xenografts using dynamic contrast-enhanced computed tomography. *Int J Radiat Oncol Biol Phys* 2014;88:412-418.
19. Mains JR, Donskov F, Pedersen E, et al. Dynamic contrast-enhanced computed tomography as a potential biomarker in patients with metastatic renal cell carcinoma: Preliminary results from the Danish Renal Cancer Group Study-1. *Invest Radiol* 2014;49:601-607.
20. Coolens C, Driscoll B, Moseley J, et al. Feasibility of 4D perfusion CT imaging for the assessment of liver treatment response following SBRT and sorafenib. *Adv Radiat Oncol* 2016;1:194-203.
21. Coolens C, Driscoll B, Chung C, et al. Automated voxel-based analysis of volumetric dynamic contrast-enhanced CT data improves measurement of serial changes in tumor vascular biomarkers. *Int J Radiat Oncol Biol Phys* 2015;91:48-57.
22. Lazanyi KS, Abramyan A, Wolf G, et al. Usefulness of dynamic contrast enhanced computed tomography in patients with non-small-cell lung cancer scheduled for radiation therapy. *Lung Cancer* 2010; 70:280-285.
23. Wang J, Wu N, Cham MD, et al. Tumor response in patients with advanced non-small cell lung cancer: Perfusion CT evaluation of chemotherapy and radiation therapy. *Am J Roentgenol* 2009;193: 1090-1096.
24. Koh TS, Ng QS, Thng CH, et al. Primary colorectal cancer: Use of kinetic modeling of dynamic contrast-enhanced CT data to predict clinical outcome. *Radiology* 2013;267:145-154.
25. Gillies RJ, Kinahan PE, Hricak H. Radiomics: Images are more than pictures, they are data. *Radiology* 2016;278:563-577.
26. Lambin P, Rios-Velazquez E, Leijenaar R, et al. Radiomics: Extracting more information from medical images using advanced feature analysis. *Eur J Cancer* 2012;48:441-446.
27. Parmar C, Rios-Velazquez E, Leijenaar R, et al. Radiomic feature clusters and prognostic signatures specific for lung and head & neck cancer. *Sci Rep* 2015;5:11044.
28. Coroller TP, Grossmann P, Hou Y, et al. CT-based radiomic signature predicts distant metastasis in lung adenocarcinoma. *Radiother Oncol* 2015;114:345-350.
29. Aerts HJ, Velazquez ER, Leijenaar RT, et al. Decoding tumour phenotype by noninvasive imaging using a quantitative radiomics approach. *Nat Commun* 2014;5:4006.
30. Huynh E, Coroller TP, Narayan V, et al. CT-based radiomic analysis of stereotactic body radiation therapy patients with lung cancer. *Radiother Oncol* 2016;120:258-266.
31. Yu W, Tang C, Hobbs BP, et al. Development and validation of a predictive radiomics model for clinical outcomes in stage I non-small cell lung cancer. *Int J Radiat Oncol Biol Phys* 2018;102:1090-1097.
32. Li Q, Kim J, Balagurunathan Y, et al. CT imaging features associated with recurrence in non-small cell lung cancer patients after stereotactic body radiotherapy. *Radiat Oncol* 2017;12:158.
33. Coroller TP, Agrawal V, Huynh E, et al. Radiomic-based pathological response prediction from primary tumors and lymph nodes in NSCLC. *J Thorac Oncol* 2017;12:467-476.
34. Coroller TP, Agrawal V, Narayan V, et al. Radiomic phenotype features predict pathological response in non-small cell lung cancer. *Radiother Oncol* 2016;119:480-486.
35. Fave X, Yang J, MacKin D, et al. Delta-radiomics features for the prediction of patient outcomes in non-small cell lung cancer. *Sci Rep* 2017;7:588.
36. Balagurunathan Y, Gu Y, Wang H, et al. Reproducibility and prognosis of quantitative features extracted from CT images. *Transl Oncol* 2014;7:72-87.
37. Kalpathy-Cramer J, Mamomov A, Zhao B, et al. Radiomics of lung nodules: A multi-institutional study of robustness and agreement of quantitative imaging features. *Tomography* 2016;2:430-437.
38. Rubin DL, Willrell D, O'Connor M, et al. Automated tracking of quantitative assessments of tumor burden in clinical trials. *Transl Oncol* 2014;7:23-35.
39. Velazquez ER, Willrett D, O'Connor M, et al. Volumetric CT-based segmentation of NSCLC using 3D-Slicer. *Sci Rep* 2013;3:3529.
40. Kalpathy-Cramer J, Zhao B, Goldgof D, et al. A comparison of lung nodule segmentation algorithms: Methods and results from a multi-institutional study. *J Digit Imaging* 2016;29:476-487.
41. Hallqvist A, Alverbratta C, Strandell B, et al. Positron emission tomography and computed tomographic imaging (PET/CT) for dose planning purposes of thoracic radiation with curative intent in lung cancer patients: A systematic review and meta-analysis. *Radiother Oncol* 2017;123:71-77.
42. van Loon J, De Ruysscher D, Wanders R, et al. Selective nodal irradiation on basis of (18)FDG-PET scans in limited-disease small-cell lung cancer: A prospective study. *Int J Radiat Oncol Biol Phys* 2010;77:329-336.
43. Taghipour M, Bey A, Arous F, et al. Use of 18F-Fludeoxyglucose-positron emission tomography/computed tomography for patient management and outcome in oropharyngeal squamous cell carcinoma: A review. *JAMA Otolaryngol Head Neck Surg* 2016;142: 79-85.
44. Dutta PR, Riaz N, McBride S, et al. Postoperative PET/CT and target delineation before adjuvant radiotherapy in patients with oral cavity squamous cell carcinoma. *Head Neck* 2016;38(Suppl 1):E1285-E1293.
45. Li XX, Liu N-B, Zhu L, et al. Consequences of additional use of contrast-enhanced (18)F-FDG PET/CT in target volume delineation and dose distribution for pancreatic cancer. *Br J Radiol* 2015;88: 20140590.
46. Girinsky T, Aupérin A, Ribrag V, et al. Role of FDG-PET in the implementation of involved-node radiation therapy for Hodgkin lymphoma patients. *Int J Radiat Oncol Biol Phys* 2014;89:1047-1052.
47. Illidge T, Specht L, Yahalom J, et al. Modern radiation therapy for nodal non-Hodgkin lymphoma-target definition and dose guidelines from the International Lymphoma Radiation Oncology Group. *Int J Radiat Oncol Biol Phys* 2014;89:49-58.
48. Krengli M, Milia ME, Turri L, et al. FDG-PET/CT imaging for staging and target volume delineation in conformal radiotherapy of anal carcinoma. *Radiat Oncol* 2010;5:10.
49. Whaley JT, Fernandes AT, Robert Sackmann R, et al. Clinical utility of integrated positron emission tomography/computed tomography imaging in the clinical management and radiation treatment planning of locally advanced rectal cancer. *Pract Radiat Oncol* 2014;4: 226-232.
50. Schinagl DA, Vogel WV, Hoffmann AL, et al. Comparison of five segmentation tools for 18F-fluoro-deoxy-glucose-positron emission tomography-based target volume definition in head and neck cancer. *Int J Radiat Oncol Biol Phys* 2007;69:1282-1289.
51. Beichel RR, Smith BJ, Bauer C, et al. Multi-site quality and variability analysis of 3D FDG PET segmentations based on phantom and clinical image data. *Med Phys* 2017;44:479-496.
52. Jeganathan R, McGuigan J, Campbell F, et al. Does pre-operative estimation of oesophageal tumour metabolic length using 18F-fluorodeoxyglucose PET/CT images compare with surgical pathology length? *Eur J Nucl Med Mol Imaging* 2011;38:656-662.
53. Hatt M, Lee JA, Charles R, et al. Classification and evaluation strategies of auto-segmentation approaches for PET: Report of AAPM task group No. 211. *Med Phys* 2017;44:e1-e42.
54. Lupi A, Salgarello M, Malfatti V, et al. The effect of 18F-FDG-PET/CT respiratory gating on detected metabolic activity in lung lesions. *Ann Nucl Med* 2009;23:191-196.

55. Brock KK, Mutic S, McNutt TR, et al. Use of image registration and fusion algorithms and techniques in radiotherapy: Report of the AAPM Radiation Therapy Committee Task Group No. 132. *Med Phys* 2017;44:e43-e76.
56. Jeraj R, Bradshaw T, Simoncic U. Molecular imaging to plan radiotherapy and evaluate its efficacy. *J Nucl Med* 2015;56:1752-1765.
57. Lordick F, Ott K, Krause BJ, et al. PET to assess early metabolic response and to guide treatment of adenocarcinoma of the oesophagogastric junction: The MUNICON phase II trial. *Lancet Oncol* 2007;8:797-805.
58. Goodman KA, Niedzwiecki D, Hall N, et al. Initial results of CALGB 80803 (Alliance): A randomized phase II trial of PET scan-directed combined modality therapy for esophageal cancer. *J Clin Oncol* 2017;35:1.
59. Jin S, Kim S-B, Ahn J-H, et al. 18 F-fluorodeoxyglucose uptake predicts pathological complete response after neoadjuvant chemotherapy for breast cancer: A retrospective cohort study. *J Surg Oncol* 2013;107:180-187.
60. Martoni AA, Zamagni C, Quercia S, et al. Early (18)F-2-fluoro-2-deoxy-d-glucose positron emission tomography may identify a subset of patients with estrogen receptor-positive breast cancer who will not respond optimally to preoperative chemotherapy. *Cancer* 2010; 116:805-813.
61. Humbert O, Berriolo A, Riedinger M, et al. Changes in 18F-FDG tumor metabolism after a first course of neoadjuvant chemotherapy in breast cancer: Influence of tumor subtypes. *Ann Oncol* 2012;23: 2572-2577.
62. Coudert B, Pierga J-Y, Mouret-Reynier M-A, et al. Use of [(18)F]-FDG PET to predict response to neoadjuvant trastuzumab and docetaxel in patients with HER2-positive breast cancer, and addition of bevacizumab to neoadjuvant trastuzumab and docetaxel in [(18)F]-FDG PET-predicted non-responders (AVATAHER): An open-label, randomised phase 2 trial. *Lancet Oncol* 2014;15:1493-1502.
63. Kong FM, Frey KA, Quint LE, et al. A pilot study of [18F]fluorodeoxyglucose positron emission tomography scans during and after radiation-based therapy in patients with non small-cell lung cancer. *J Clin Oncol* 2007;25:3116-3123.
64. van Baardwijk A, Bosmans G, Dekkera A, et al. Time trends in the maximal uptake of FDG on PET scan during thoracic radiotherapy. A prospective study in locally advanced non-small cell lung cancer (NSCLC) patients. *Radiother Oncol* 2007;82:145-152.
65. van Elmpet W, Öllers M, Dingemans AC, et al. Response assessment using 18F-FDG PET early in the course of radiotherapy correlates with survival in advanced-stage non-small cell lung cancer. *J Nucl Med* 2012;53:1514-1520.
66. Krhili S, Muratet JP, Roche S, et al. Use of metabolic parameters as prognostic factors during concomitant chemoradiotherapy for locally advanced cervical cancer. *Am J Clin Oncol* 2017;40:250-255.
67. Kidd EA, Thomas M, Siegel BA, et al. Changes in cervical cancer FDG uptake during chemoradiation and association with response. *Int J Radiat Oncol Biol Phys* 2013;85:116-122.
68. Janssen MH, Öllers MC, van Stiphout R, et al. Evaluation of early metabolic responses in rectal cancer during combined radio-chemotherapy or radiotherapy alone: Sequential FDG-PET-CT findings. *Radiother Oncol* 2010;94:151-155.
69. Hentschel M, Appold S, Schreiber A, et al. Early FDG PET at 10 or 20 Gy under chemoradiotherapy is prognostic for locoregional control and overall survival in patients with head and neck cancer. *Eur J Nucl Med Mol Imaging* 2011;38:1203-1211.
70. Higashi K, Clavo AC, Wahl RL. In vitro assessment of 2-fluoro-2-deoxy-D-glucose, L-methionine and thymidine as agents to monitor the early response of a human adenocarcinoma cell line to radiotherapy. *J Nucl Med* 1993;34:773-779.
71. Kong FM, Ten Haken RK, Schipper M, et al. Effect of midtreatment PET/CT-adapted radiation therapy with concurrent chemotherapy in patients with locally advanced non-small-cell lung cancer: A phase 2 clinical trial. *JAMA Oncol* 2017;3:1358-1365.
72. Cremonesi M, Gilardi L, Ferrari ME, et al. Role of interim 18F-FDG-PET/CT for the early prediction of clinical outcomes of non-small cell lung cancer (NSCLC) during radiotherapy or chemoradiotherapy. A systematic review. *Eur J Nucl Med Mol Imaging* 2017;44:1915-1927.
73. Minn H, Zasadny KR, Quint LE, et al. Lung cancer: Reproducibility of quantitative measurements for evaluating 2-[F-18]-fluoro-2-deoxy-D-glucose uptake at PET. *Radiology* 1995;196:167-173.
74. Lockhart CM, MacDonald LR, Alessio AM, et al. Quantifying and reducing the effect of calibration error on variability of PET/CT standardized uptake value measurements. *J Nucl Med* 2011;52: 218-224.
75. Kurland BF, Muzy M, Peterson LM, et al. Multicenter clinical trials using 18F-FDG PET to measure early response to oncologic therapy: Effects of injection-to-acquisition time variability on required sample size. *J Nucl Med* 2016;57:226-230.
76. Boellaard R, Delgado-Bolton R, Oyen WJG, et al. FDG PET/CT: EANM procedure guidelines for tumour imaging: Version 2.0. *Eur J Nucl Med Mol Imaging* 2015;42:328-354.
77. Ulrich EJ, Sunderland JJ, Smith BJ, et al. Automated model-based quantitative analysis of phantoms with spherical inserts in FDG PET scans. *Med Phys* 2018;45:258-276.
78. Scheuermann JS, Reddin JS, Opanowski A, et al. Qualification of National Cancer Institute-designated cancer centers for quantitative PET/CT imaging in clinical trials. *J Nucl Med* 2017;58:1065-1071.
79. Smith BJ, Beichel RR. A Bayesian framework for performance assessment and comparison of imaging biomarker quantification methods. *Stat Methods Med Res* 2017. 962280217741334.
80. Young H, Baum R, Cremerius U, et al. Measurement of clinical and subclinical tumour response using [18F]-fluorodeoxyglucose and positron emission tomography: Review and 1999 EORTC recommendations. *Eur J Cancer* 1999;35:1773-1782.
81. Wahl RL, Jacene H, Kasamon Y, et al. From RECIST to PERCIST: Evolving considerations for PET response criteria in solid tumors. *J Nucl Med* 2009;50(Suppl 1):122S-150S.
82. Leal J, Wahl R. Auto-PERCIST™: A semi-automated system for response assessment based on the PERCIST 1.0 criteria for quantitative analysis of FDG PET. *J Nuclear Medicine* 2014;55:1368.
83. Tahari AK, Chien D, Azadi JR, et al. Optimum lean body formulation for correction of standardized uptake value in PET imaging. *J Nucl Med* 2014;55:1481-1484.
84. Lodge MA, Chaudhry MA, Wahl RL. Noise considerations for PET quantification using maximum and peak standardized uptake value. *J Nucl Med* 2012;53:1041-1047.
85. Mansor S, Pfahler E, Heijtel D, et al. Impact of PET/CT system, reconstruction protocol, data analysis method, and repositioning on PET/CT precision: An experimental evaluation using an oncology and brain phantom. *Med Phys* 2017;44:6413-6424.
86. Hill RP, Bristow RG, Fyles A, et al. Hypoxia and predicting radiation response. *Semin Radiat Oncol* 2015;25:260-272.
87. Kallinowski F, Zander R, Hoeckel M, et al. Tumor tissue oxygenation as evaluated by computerized-pO2-histogram. *Int J Radiat Oncol Biol Phys* 1990;19:953-961.
88. Rasey JS, Grunbaum Z, Magee S, et al. Characterization of radio-labeled fluoromisonidazole as a probe for hypoxic cells. *Radiat Res* 1987;111:292-304.
89. Mortensen LS, Johansen J, Kallehauge J, et al. FAZA PET/CT hypoxia imaging in patients with squamous cell carcinoma of the head and neck treated with radiotherapy: Results from the DAHANCA 24 trial. *Radiother Oncol* 2012;105:14-20.
90. Sorger D, Patta M, Kumard P, et al. [18F]Fluoroazomycinarabinofuranoside (18 FAZA) and [18F]Fluoromisonidazole (18FMISO): A comparative study of their selective uptake in hypoxic cells and PET imaging in experimental rat tumors. *Nucl Med Biol* 2003;30:317-326.
91. Dubois LJ, Lieuwes NG, Janssen MHM, et al. Preclinical evaluation and validation of [18F]HX4, a promising hypoxia marker for PET imaging. *Proc Natl Acad Sci U S A* 2011;108:14620-14625.

92. Lewis JS, McCarthy DW, McCarthy TJ, et al. Evaluation of 64Cu-ATSM in vitro and in vivo in a hypoxic tumor model. *J Nucl Med* 1999;40:177-183.
93. Parker C, Milosevic M, Toi A, et al. Polarographic electrode study of tumor oxygenation in clinically localized prostate cancer. *Int J Radiat Oncol Biol Phys* 2004;58:750-757.
94. Dhani NC, Serra S, Pintilie M, et al. Analysis of the intra- and intertumoral heterogeneity of hypoxia in pancreatic cancer patients receiving the nitroimidazole tracer pimonidazole. *Br J Cancer* 2015; 113:864.
95. Rischin D, Hicks RJ, Fisher R, et al. Prognostic significance of [18F]-misonidazole positron emission tomography-detected tumor hypoxia in patients with advanced head and neck cancer randomly assigned to chemoradiation with or without tirapazamine: A substudy of Trans-Tasman Radiation Oncology Group Study 98.02. *J Clin Oncol* 2006;24:2098-2104.
96. Zips D, Zöphel K, Abolmaali N, et al. Exploratory prospective trial of hypoxia-specific PET imaging during radiochemotherapy in patients with locally advanced head-and-neck cancer. *Radiother Oncol* 2012;105:21-28.
97. Wiedenmann NE, Bucher S, Hentschel M, et al. Serial [18F]-fluoromisonidazole PET during radiochemotherapy for locally advanced head and neck cancer and its correlation with outcome. *Radiother Oncol* 2015;117:113-117.
98. Gerstner ER, Zhang Z, Fink JR, et al. ACRIN 6684: Assessment of tumor hypoxia in newly diagnosed glioblastoma using 18F-FMISO PET and MRI. *Clin Cancer Res* 2016;22:5079-5086.
99. Spence AM, Muzi M, Swanson KR, et al. Regional hypoxia in glioblastoma multiforme quantified with [18F]Fluoromisonidazole positron emission tomography before radiotherapy: Correlation with time to progression and survival. *Clin Cancer Res* 2008;14:2623-2630.
100. Brustugun OT. Hypoxia as a cause of treatment failure in non-small cell carcinoma of the lung. *Semin Radiat Oncol* 2015;25:87-92.
101. Kinoshita T, Fujii H, Hayashi Y, et al. Prognostic significance of hypoxic PET using (18)F-FAZA and (62)Cu-ATSM in non-small-cell lung cancer. *Lung Cancer* 2016;91:56-66.
102. Fyles A, Milosevic M, Hedley D, et al. Tumor hypoxia has independent predictor impact only in patients with node-negative cervix cancer. *J Clin Oncol* 2002;20:680-687.
103. Milosevic M, Warde P, Ménard C, et al. Tumor hypoxia predicts biochemical failure following radiotherapy for clinically localized prostate cancer. *Clin Cancer Res* 2012;18:2108-2114.
104. Bittner MI, Wiedenmann N, Bucher S, et al. Exploratory geographical analysis of hypoxic subvolumes using 18F-MISO-PET imaging in patients with head and neck cancer in the course of primary chemoradiotherapy. *Radiother Oncol* 2013;108:511-516.
105. Bollineni VR, Wiegman EM, Pruim J, et al. Hypoxia imaging using positron emission tomography in non-small cell lung cancer: Implications for radiotherapy. *Cancer Treat Rev* 2012;38:1027-1032.
106. Horsman MR, Mortensen LS, Petersen JB, et al. Imaging hypoxia to improve radiotherapy outcome. *Nat Rev Clin Oncol* 2012;9:674-687.
107. Welz S, Mönnich D, Pfannenberg C, et al. Prognostic value of dynamic hypoxia PET in head and neck cancer: Results from a planned interim analysis of a randomized phase II hypoxia-image guided dose escalation trial. *Radiother Oncol* 2017;24:526-532.
108. Pigorsch SU, Wilkens JJ, Kampfer S, et al. Do selective radiation dose escalation and tumour hypoxia status impact the loco-regional tumour control after radio-chemotherapy of head & neck tumours? The ESCALOX protocol. *Radiat Oncol* 2017;12:45.
109. National Cancer Institute Cancer Imaging Program. Princess Margaret Cancer Centre, Toronto, Canada: Image-based quantitative assessment of tumor hypoxia. Available at: https://imaging.cancer.gov/programs_resources/specialized_initiatives/qjin/qinsites/university_health_network.htm. Accessed December 1, 2017.
110. Muzi M, Peterson LM, O'Sullivan JN, et al. 18F-Fluoromisonidazole quantification of hypoxia in human cancer patients using image-derived blood surrogate tissue reference regions. *J Nucl Med* 2015; 56:1223-1228.
111. Taylor E, Yeung I, Keller H, et al. Quantifying hypoxia in human cancers using static PET imaging. *Phys Med Biol* 2016;61:7957-7974.
112. Muzi M, Krohn KA. Imaging Hypoxia with (1)(8)F-Fluoromisonidazole: Challenges in moving to a more complicated analysis. *J Nucl Med* 2016;57:497-498.
113. Grkovski M, Schöder H, Lee NY, et al. Multiparametric imaging of tumor hypoxia and perfusion with 18F-fluoromisonidazole dynamic PET in head and neck cancer. *J Nucl Med* 2017;58:1072-1080.
114. Taylor E, Gottwald J, Yeung I, et al. Impact of tissue transport on PET hypoxia quantification in pancreatic tumours. *EJNMMI Res* 2017;7:101.
115. Rasey JS, Grierson JR, Wiens LW, et al. Validation of FLT uptake as a measure of thymidine kinase-1 activity in A549 carcinoma cells. *J Nucl Med* 2002;43:1210-1217.
116. Lodge MA, Holdhoff M, Leal JP, et al. Repeatability of (18)F-FLT PET in a multicenter study of patients with high-grade glioma. *J Nucl Med* 2017;58:393-398.
117. Rendl G, Rettenbacher L, Holzmannhofer J, et al. Assessment of response to neoadjuvant radiochemotherapy with F-18 FLT and F-18 FDG PET/CT in patients with rectal cancer. *Ann Nucl Med* 2015;29: 284-294.
118. Trigonis I, Koh PK, Ben Taylor B, et al. Early reduction in tumour [18F]fluorothymidine (FLT) uptake in patients with non-small cell lung cancer (NSCLC) treated with radiotherapy alone. *Eur J Nucl Med Mol Imaging* 2014;41:682-693.
119. Crandall JP, Tahari AK, Juergens RA, et al. A comparison of FLT to FDG PET/CT in the early assessment of chemotherapy response in stages IB-IIIA resectable NSCLC. *EJNMMI Res* 2017;7:8.
120. Kishino T, Hoshikawa H, Nishiyama Y, et al. Usefulness of 3'-deoxy-3'-18F-fluorothymidine PET for predicting early response to chemoradiotherapy in head and neck cancer. *J Nucl Med* 2012;53:1521-1527.
121. Hoeben BA, Troost EG, Span PN, et al. 18F-FLT PET during radiotherapy or chemoradiotherapy in head and neck squamous cell carcinoma is an early predictor of outcome. *J Nucl Med* 2013;54: 532-540.
122. Everitt S, Ball D, Hicks RJ, et al. Prospective study of serial imaging comparing fluorodeoxyglucose positron emission tomography (PET) and fluorothymidine PET during radical chemoradiation for non-small cell lung cancer: Reduction of detectable proliferation associated with worse survival. *Int J Radiat Oncol Biol Phys* 2017;99: 947-955.
123. McGuire SM, Bhatia SK, Sun W, et al. Using [(18)F]Fluorothymidine imaged with positron emission tomography to quantify and reduce hematologic toxicity due to chemoradiation therapy for pelvic cancer patients. *Int J Radiat Oncol Biol Phys* 2016;96:228-239.
124. Ackerstaff E, Glunde K, Bhujwalla ZM. Choline phospholipid metabolism: A target in cancer cells? *J Cell Biochem* 2003;90:525-533.
125. Calais J, Cao M, Nickols NG. The utility of PET/CT in external radiation therapy planning of prostate cancer. *J Nucl Med* 2018;59: 557-567.
126. van Leeuwen PJ, Stricker P, Hraby G, et al. (68) Ga-PSMA has a high detection rate of prostate cancer recurrence outside the prostatic fossa in patients being considered for salvage radiation treatment. *BJU Int* 2016;117:732-739.
127. Schuster DM, Votaw JR, Nieh PT, et al. Initial experience with the radiotracer anti-1-amino-3-18F-fluorocyclobutane-1-carboxylic acid with PET/CT in prostate carcinoma. *J Nucl Med* 2007;48:56-63.
128. Aerts HJ. The potential of radiomic-based phenotyping in precision medicine: A review. *JAMA Oncol* 2016;2:1636-1642.
129. Grossmann P, Stringfield O, El-Hachem N, et al. Defining the biological basis of radiomic phenotypes in lung cancer. *Elife* 2017;6.

130. Rios Velazquez E, Parmar C1, Liu Y, et al. Somatic mutations drive distinct imaging phenotypes in lung cancer. *Cancer Res* 2017;77:3922-3930.
131. Bogowicz M, Leijenaar RTH, Tanadini-Lang S, et al. Post-radiotherapy PET radiomics in head and neck cancer—The influence of radiomics implementation on the reproducibility of local control tumor models. *Radiother Oncol* 2017;125:385-391.
132. Lovinfosse P, Polus M, Van Daele D, et al. FDG PET/CT radiomics for predicting the outcome of locally advanced rectal cancer. *Eur J Nucl Med Mol Imaging* 2017;45:365-375.
133. Lucia F, Visvikis D, Desseroit MC, et al. Prediction of outcome using pretreatment (18)F-FDG PET/CT and MRI radiomics in locally advanced cervical cancer treated with chemoradiotherapy. *Eur J Nucl Med Mol Imaging* 2018;45:768-786.
134. Lohmann P, Stoffels G, Ceccon G, et al. Radiation injury vs. recurrent brain metastasis: Combining textural feature radiomics analysis and standard parameters may increase (18)F-FET PET accuracy without dynamic scans. *Eur Radiol* 2017;27:2916-2927.
135. Leijenaar RT, Nalbantov G, Carvalho S, et al. The effect of SUV discretization in quantitative FDG-PET radiomics: The need for standardized methodology in tumor texture analysis. *Sci Rep* 2015;5:11075.
136. Tofts PS, Brix G, Buckley D, et al. Estimating kinetic parameters from dynamic contrast-enhanced T(1)-weighted MRI of a diffusible tracer: Standardized quantities and symbols. *J Magn Reson Imaging* 1999;10:223-232.
137. Tsien C, Galbán CJ, Chenevert TL, et al. Parametric response map as an imaging biomarker to distinguish progression from pseudoprogression in high-grade glioma. *J Clin Oncol* 2010;28:2293-2299.
138. Boxerman JL, Ellingson BM, Jeyapalan S, et al. Longitudinal DSC-MRI for distinguishing tumor recurrence from pseudoprogression in patients with a high-grade glioma. *Amer J Clin Oncol* 2017;40:228-234.
139. Kuchcinski G, Le Rhun E, Cortot AB, et al. Dynamic contrast-enhanced MR imaging pharmacokinetic parameters as predictors of treatment response of brain metastases in patients with lung cancer. *Eur Radiol* 2017;27:3733-3743.
140. Yoo RE, Choi SH, Kim TM, et al. Dynamic contrast-enhanced MR imaging in predicting progression of enhancing lesions persisting after standard treatment in glioblastoma patients: A prospective study. *Eur Radiol* 2017;27:3156-3166.
141. Hatzoglou V, Yang TJ, Omuro A, et al. A prospective trial of dynamic contrast-enhanced MRI perfusion and fluorine-18 FDG PET/CT in differentiating brain tumor progression from radiation injury after cranial irradiation. *Neuro Oncol* 2016;18:873-880.
142. Shin KE, Ahn KJ, Choi HS, et al. DCE and DSC MR perfusion imaging in the differentiation of recurrent tumour from treatment-related changes in patients with glioma. *Clin Radiol* 2014;69:e264-e272.
143. Schmainda KM, Zhang Z, Prah M, et al. Dynamic susceptibility contrast MRI measures of relative cerebral blood volume as a prognostic marker for overall survival in recurrent glioblastoma: Results from the ACRIN 6677/RTOG 0625 multicenter trial. *Neuro Oncol* 2015;17:1148-1156.
144. National Cancer Institute Cancer Imaging Program. ECOG-ACRIN-Based QIN Resource for Advancing Quantitative Cancer Imaging in Clinical Trials. Available at: https://imaging.cancer.gov/programs_resources/specialized_initiatives/qin/qinsites/ecog_acrin.htm. Accessed December 1, 2017.
145. Cao Y, Popovtzer A, Li D, et al. Early prediction of outcome in advanced head-and-neck cancer based on tumor blood volume alterations during therapy: A prospective study. *Int J Radiat Oncol Biol Phys* 2008;72:1287-1290.
146. Shukla-Dave A, Lee NY, Jansen J, et al. Dynamic contrast-enhanced magnetic resonance imaging as a predictor of outcome in head-and-neck squamous cell carcinoma patients with nodal metastases. *Int J Radiat Oncol Biol Phys* 2012;82:1837-1844.
147. Kim S, Loevner LA, Quon H, et al. Prediction of response to chemoradiation therapy in squamous cell carcinomas of the head and neck using dynamic contrast-enhanced MR imaging. *Am J Neuroradiol* 2010;31:262-268.
148. Tao X, Wang L, Hui Z, et al. DCE-MRI perfusion and permeability parameters as predictors of tumor response to CCRT in patients with locally advanced NSCLC. *Sci Rep* 2016;6:35569.
149. Dijkhoff RAP, Beets-Tan RGH, Lambregts DMJ, et al. Value of DCE-MRI for staging and response evaluation in rectal cancer: A systematic review. *Eur J Radiol* 2017;95:155-168.
150. Wang P, Popovtzer A, Eisbruch A, et al. An approach to identify, from DCE MRI, significant subvolumes of tumors related to outcomes in advanced head-and-neck cancer. *Med Phys* 2012;39:5277-5285.
151. You D, Aryal M, Samuels S, et al. SU-E-J-241: Wavelet-based temporal feature extraction from DCE-MRI to identify subvolumes of low blood volume in head-and-neck cancer. *Med Phys* 2015;42:3321.
152. Prah MA, Stufflebeam SM, Paulson ES, et al. Repeatability of standardized and normalized relative CBV in patients with newly diagnosed glioblastoma. *Am J Neuroradiol* 2015;36:1654-1661.
153. Huang W, Chen Y, Fedorov A, et al. The impact of arterial input function determination variations on prostate dynamic contrast-enhanced magnetic resonance imaging pharmacokinetic modeling: A multicenter data analysis challenge. *Tomography* 2016;2:56-66.
154. Farjam R, Tsien CI, Feng FY, et al. Investigation of the diffusion abnormality index as a new imaging biomarker for early assessment of brain tumor response to radiation therapy. *Neuro Oncol* 2014;16:131-139.
155. Vandecaveye V, Dirix P, De Keyzer F, et al. Diffusion-weighted magnetic resonance imaging early after chemoradiotherapy to monitor treatment response in head-and-neck squamous cell carcinoma. *Int J Radiat Oncol Biol Phys* 2012;82:1098-1107.
156. van Rossum PS, van Lier AL, van Vulpen M, et al. Diffusion-weighted magnetic resonance imaging for the prediction of pathologic response to neoadjuvant chemoradiotherapy in esophageal cancer. *Radiother Oncol* 2015;115:163-170.
157. Liu L, Wu N, Ouyang H, et al. Diffusion-weighted MRI in early assessment of tumour response to radiotherapy in high-risk prostate cancer. *Br J Radiol* 2014;87:20140359.
158. Tshering Vogel DW, Zbaeren P, Geretschlaeger A, et al. Diffusion-weighted MR imaging including bi-exponential fitting for the detection of recurrent or residual tumour after (chemo)radiotherapy for laryngeal and hypopharyngeal cancers. *Eur Radiol* 2013;23:562-569.
159. Vandecaveye V, De Keyzer F, Nuyts S, et al. Detection of head and neck squamous cell carcinoma with diffusion weighted MRI after (chemo)radiotherapy: Correlation between radiologic and histopathologic findings. *Int J Radiat Oncol Biol Phys* 2007;67:960-971.
160. Becker M, Varoquaux AD, Combescure C, et al. Local recurrence of squamous cell carcinoma of the head and neck after radio(chemo)therapy: Diagnostic performance of FDG-PET/MRI with diffusion-weighted sequences. *Eur Radiol* 2018;28:651-663.
161. Roy C, Foudi F, Charton J, et al. Comparative sensitivities of functional MRI sequences in detection of local recurrence of prostate carcinoma after radical prostatectomy or external-beam radiotherapy. *Am J Roentgenol* 2013;200:W361-W368.
162. Morgan VA, Riches SF, Giles S, et al. Diffusion-weighted MRI for locally recurrent prostate cancer after external beam radiotherapy. *Am J Roentgenol* 2012;198:596-602.
163. Kim CK, Park BK, Kim B. High-b-value diffusion-weighted imaging at 3 T to detect prostate cancer: Comparisons between b values of 1,000 and 2,000 s/mm². *Am J Roentgenol* 2010;194:W33-W37.
164. Woo S, Suh CH, Kim SY, et al. Head-to-head comparison between high- and standard-b-value DWI for detecting prostate cancer: A systematic review and meta-analysis. *Am J Roentgenol* 2017;1-10.

165. Godley KC, Syer TJ, Toms AP, et al. Accuracy of high b-value diffusion-weighted MRI for prostate cancer detection: A meta-analysis. *Acta Radiol* 2017; 284185117702181.
166. Yuan Q, Costa DN, Sénégas J, et al. Quantitative diffusion-weighted imaging and dynamic contrast-enhanced characterization of the index lesion with multiparametric MRI in prostate cancer patients. *J Magn Reson Imaging* 2017;45:908-916.
167. Kitajima K, Takahashi S, Ueno Y, et al. Do apparent diffusion coefficient (ADC) values obtained using high b-values with a 3-T MRI correlate better than a transrectal ultrasound (TRUS)-guided biopsy with true Gleason scores obtained from radical prostatectomy specimens for patients with prostate cancer? *Eur J Radiol* 2013;82:1219-1226.
168. Kido A, Kim CK, Par SY, et al. Incremental value of high b value diffusion-weighted magnetic resonance imaging at 3 T for prediction of extracapsular extension in patients with prostate cancer: Preliminary experience. *Radiol Med* 2017;122:228-238.
169. Newitt DC, Malyarenko D, Chenevert TL, et al. Multisite concordance of apparent diffusion coefficient measurements across the NCI Quantitative Imaging Network. *J Med Imaging (Bellingham)* 2018;5: 011003.
170. Garcia-Gomez JM, Luts J, Julià-Sapé M, et al. Multiproject-multi-center evaluation of automatic brain tumor classification by magnetic resonance spectroscopy. *MAGMA* 2009;22:5-18.
171. Li Y, Lupo JM, Parvataneni R, et al. Survival analysis in patients with newly diagnosed glioblastoma using pre- and postradiotherapy MR spectroscopic imaging. *Neuro Oncol* 2013;15:607-617.
172. Deviers A, Ken S, Filleron T, et al. Evaluation of the lactate-to-N-acetyl-aspartate ratio defined with magnetic resonance spectroscopic imaging before radiation therapy as a new predictive marker of the site of relapse in patients with glioblastoma multiforme. *Int J Radiat Oncol Biol Phys* 2014;90:385-393.
173. Muruganandham M, Clerkin PP, Smith BJ, et al. 3-dimensional magnetic resonance spectroscopic imaging at 3 tesla for early response assessment of glioblastoma patients during external beam radiation therapy. *Int J Radiat Oncol Biol Phys* 2014;90:181-189.
174. Huang J, Wang AM, Shetty A, et al. Differentiation between intra-axial metastatic tumor progression and radiation injury following fractionated radiation therapy or stereotactic radiosurgery using MR spectroscopy, perfusion MR imaging or volume progression modeling. *Magn Reson Imaging* 2011;29:993-1001.
175. Park I, Tamai G, Lee MC, et al. Patterns of recurrence analysis in newly diagnosed glioblastoma multiforme after three-dimensional conformal radiation therapy with respect to pre-radiation therapy magnetic resonance spectroscopic findings. *Int J Radiat Oncol Biol Phys* 2007;69:381-389.
176. Laprie A, Catalaa I, Emmanuelle Cassol E, et al. Proton magnetic resonance spectroscopic imaging in newly diagnosed glioblastoma: predictive value for the site of postradiotherapy relapse in a prospective longitudinal study. *Int J Radiat Oncol Biol Phys* 2008;70:773-781.
177. Cordova JS, Kandula S, Gurbani S, et al. Simulating the effect of spectroscopic MRI as a metric for radiation therapy planning in patients with glioblastoma. *Tomography* 2016;2:366-373.
178. Parra NA, Maudsley AA, Gupta RK, et al. Volumetric spectroscopic imaging of glioblastoma multiforme radiation treatment volumes. *Int J Radiat Oncol Biol Phys* 2014;90:376-384.
179. Emir UE, Larkin SJ, de Pennington N, et al. Noninvasive quantification of 2-hydroxyglutarate in human gliomas with IDH1 and IDH2 mutations. *Cancer Res* 2016;76:43-49.
180. Ken S, Vieillevigne L, Franceris X, et al. Integration method of 3D MR spectroscopy into treatment planning system for glioblastoma IMRT dose painting with integrated simultaneous boost. *Radiat Oncol* 2013;8:1.
181. Mueller-Lisse UG, Scherr MK. Proton MR spectroscopy of the prostate. *Eur J Radiol* 2007;63:351-360.
182. Valentini AL, Gui B, D'Agostino GR, et al. Locally advanced prostate cancer: Three-dimensional magnetic resonance spectroscopy to monitor prostate response to therapy. *Int J Radiat Oncol Biol Phys* 2012;84:719-724.
183. Westphalen AC, Coakley FV, Roach M 3rd, et al. Locally recurrent prostate cancer after external beam radiation therapy: Diagnostic performance of 1.5-T endorectal MR imaging and MR spectroscopic imaging for detection. *Radiology* 2010;256:485-492.
184. Zhang VY, Westphalen A, Delos Santos L, et al. The role of metabolic imaging in radiation therapy of prostate cancer. *NMR Biomed* 2014;27:100-111.
185. Arrayeh E, Westphalen AC, Kurhanewicz J, et al. Does local recurrence of prostate cancer after radiation therapy occur at the site of primary tumor? Results of a longitudinal MRI and MRSI study. *Int J Radiat Oncol Biol Phys* 2012;82:e787-e793.
186. Nguyen ML, Willows B, Khan R, et al. The potential role of magnetic resonance spectroscopy in image-guided radiotherapy. *Front Oncol* 2014;4:91.
187. King MT, Nasser NJ, Mathur N, et al. Long-term outcome of magnetic resonance spectroscopic image-directed dose escalation for prostate brachytherapy. *Brachytherapy* 2016;15:266-273.
188. Crook J, Ots A, Gaztañaga M, et al. Ultrasound-planned high-dose-rate prostate brachytherapy: Dose painting to the dominant intraprostatic lesion. *Brachytherapy* 2014;13:433-441.
189. Parekh VS, Jacobs MA. Integrated radiomic framework for breast cancer and tumor biology using advanced machine learning and multiparametric MRI. *NPJ Breast Cancer* 2017;3:43.
190. Tiwari P, Prasanna P, Wolansky L, et al. Computer-extracted texture features to distinguish cerebral radionecrosis from recurrent brain tumors on multiparametric MRI: A feasibility study. *Am J Neuro-radiol* 2016;37:2231-2236.
191. Zhang Z, Yang J, Ho A, et al. A predictive model for distinguishing radiation necrosis from tumour progression after gamma knife radiosurgery based on radiomic features from MR images. *Eur Radiol* 2018;28:2255-2263.
192. Akkus Z, Galimzianova A, Hoog A, et al. Deep learning for brain MRI segmentation: State of the art and future directions. *J Digit Imaging* 2017;30:449-459.
193. Cordova JS, Schreibmann E, Hadjipanayis CG, et al. Quantitative tumor segmentation for evaluation of extent of glioblastoma resection to facilitate multisite clinical trials. *Transl Oncol* 2014;7: 40-47.
194. McGarry SD, Hurrell SL, Kaczmarowski AL, et al. Magnetic resonance imaging-based radiomic profiles predict patient prognosis in newly diagnosed glioblastoma before therapy. *Tomography* 2016;2: 223-228.
195. Kickingereder P, Neuberger U, Bonekamp D, et al. Radiomic subtyping improves disease stratification beyond key molecular, clinical and standard imaging characteristics in patients with glioblastoma. *Neuro Oncol* 2018;20:848-857.
196. Stoyanova R, Pollack A, Takhar M, et al. Association of multiparametric MRI quantitative imaging features with prostate cancer gene expression in MRI-targeted prostate biopsies. *Oncotarget* 2016; 7:53362-53376.
197. Chang K, Bai HX, Hao Zhou H, et al. Residual convolutional neural network for determination of IDH status in low- and high-grade gliomas from MR imaging. *Clin Cancer Res* 2018;24:1073-1081.
198. Stoyanova R, Takhar M, Tschudi Y, et al. Prostate cancer radiomics and the promise of radiogenomics. *Transl Cancer Res* 2016; 5:432-447.
199. Shiradkar R, Podder TK, Algohary A, et al. Radiomics based targeted radiotherapy planning (Rad-TRaP): A computational framework for prostate cancer treatment planning with MRI. *Radiat Oncol* 2016;11: 148.